Cell Reports Medicine, Volume *5*

Supplemental information

Potent human monoclonal antibodies targeting Epstein-Barr virus gp42 reveal vulnerable sites for virus infection

Ge-Xin Zhao, Xin-Yan Fang, Guo-Long Bu, Shuai-Jia-Bin Chen, Cong Sun, Ting Li, Chu Xie, Yu Wang, Shu-Xin Li, Ning Meng, Guo-Kai Feng, Qian Zhong, Xiang-Wei Kong, Zheng Liu, and Mu-Sheng Zeng

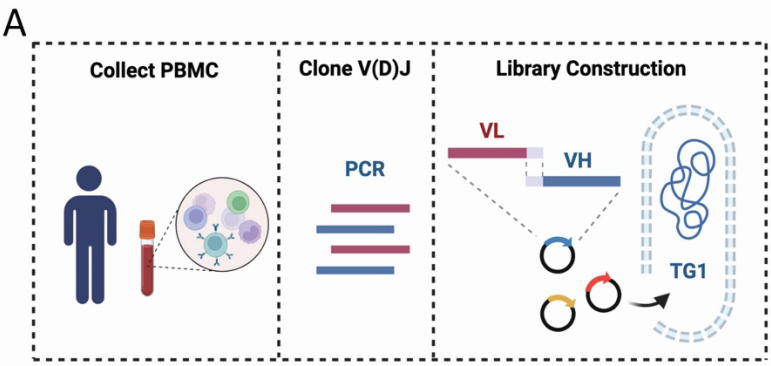

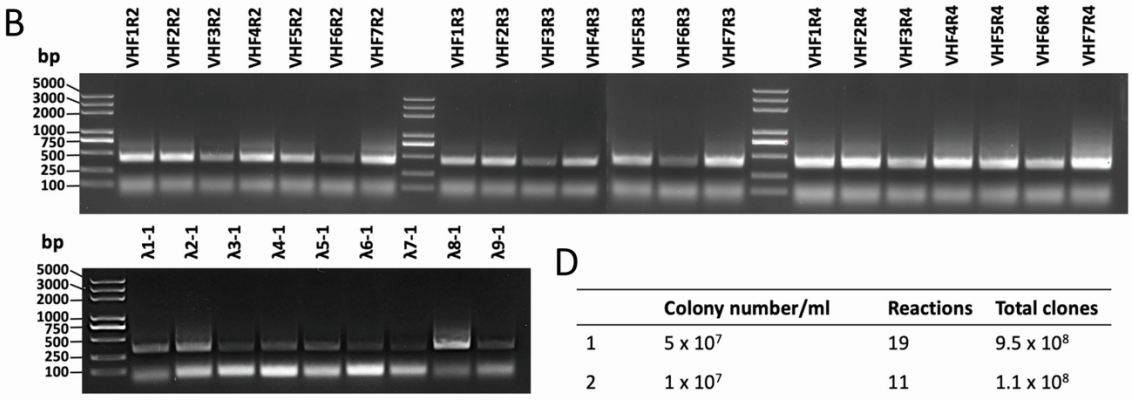

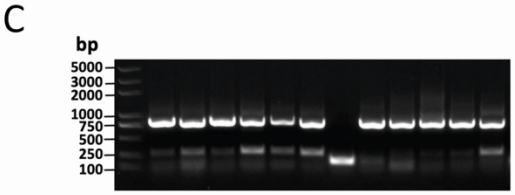

D

	Colony number/ml	Reactions	Total clones
1	5 x 10^7	19	9.5 x 10^8
2	1 x 10^7	11	1.1 x 10^8
3	1.5 x 10^7	20	3 x 10^8
4	4 x 10^7	18	7.2 x 10^8
5	5 x 10^6	20	1 x 10^8
6	3.5 x 10^7	20	7 x 10^8
Total		108	2.9 x 10^9

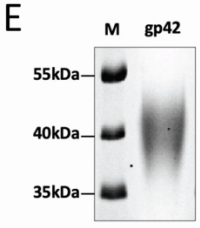

F

Round	gp42 phage titer	BSA control titer	Phage titer ratio
1st	1.3 x 10^8	1.24 x 10^8	1.04
2nd	24 x 10^8	1.8 x 10^8	13.33
3rd	188 x 10^8	1.4 x 10^8	134.29

H

% Identity	2B7 H	2C1 H	2C5 H	2D5 H
2B7 H				
2C1 H	77.428			
2C5 H	77.953	97.917		
2D5 H	77.428	98.958	98.958	

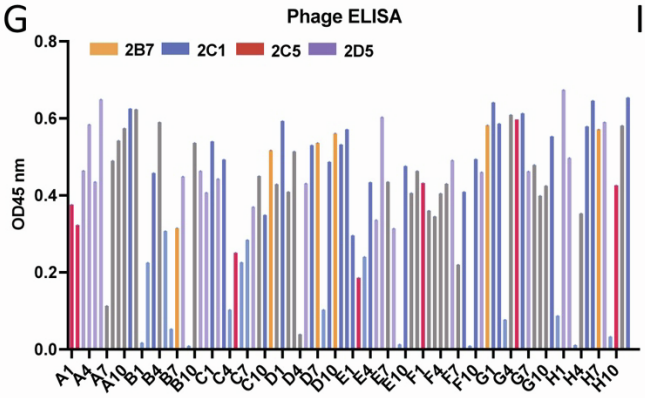

I

Ligand	Analyte	K_{on}($M^{-1}S^{-1}$)	K_{off}(S^{-1})	KD(nM)
gp42	2B7 Fab	5.562*10^6	6.253*10^3	11.241
gp42	2B7 mAb	2.792*10^5	5.834*10^{-7}	0.002
gp42	2C1 Fab	1.146*10^6	2.163*10^{-3}	1.888
gp42	2C1 mAb	6.307*10^5	3.589*10^{-4}	0.569
gH/gL/gp42	2B7 Fab	1.231*10^6	7.690*10^{-3}	6.245
gH/gL/gp42	2B7 mAb	1.125*10^6	6.672*10^{-7}	<0.001
gH/gL/gp42	2C1 Fab	1.449*10^5	2.627*10^{-3}	18.134
gH/gL/gp42	2C1 mAb	5.321*10^4	2.390*10^{-4}	4.492

Figure S1. Isolation and identification of high-affinity anti-gp42 antibodies. Related to Figure 1.

(A) The strategy of the construction of the human scfv phage library. V(D)J sequences encoding the variable regions of the heavy and light chains (vH and vL) are amplified from human PBMC. These sequences are then assembled as vL-vH using overlap PCR, inserted into the pComb3XSS vector, and introduced into E. coli (TG1 stain) using electroporation.

(B) Representative DNA gel image of vH and vL PCR products amplified from cDNA, which is reverse transcribed from RNA extracted from PBMCs of EBV-positive volunteers.

(C) Represent DNA gel image of the PCR amplification of vL-vH inserts from randomly selected TG1 clones of the scfv library. A product of about 750bp indicated that the E.coli TG1 containing the pComb3xss plasmid is successfully inserted with the vL-vH gene. The insertion rate is greater than 90% for each electroporation reaction.

(D) The efficiency of electroporation reactions (colony number/ml) was estimated by serial dilution of electroporated TG1. Six batches of electroporation for a total of 108 reactions were performed, resulting in an estimated library capacity of approximately 2.9×10^9.

(E) SDS-PAGE analysis of purified soluble gp42(34-223 aa). The protein was stained with Coomassie blue.

(F) Phage titers obtained from successive rounds of screening assessed through serial dilution of recovered-phage-infected TG1 cells on an ampicillin-containing agar plate. The phage titer ratio was determined by dividing the phage count from gp42-bound tubes by that from BSA-bound tubes. After three panning rounds, gp42-bound phages were eluted, infecting TG1 cells for subsequent ELISA screening.

(G) The affinity of individual phage clones to gp42 was detected using ELISA and sequenced. Differently colored symbols indicate distinct clones, while gray represents instances of failed sequencing, typically due to double peaks.

(H) Nucleotide sequence identity (%) of the heavy chain of 2B7, 2C1, 2C5, and 2D5.

(I) Bio-Layer Interferometry (BLI) measurements of apparent and binding affinities between gp42-specific antibodies/Fabs, and immobilized gp42 or the gH/gL/gp42 complex.

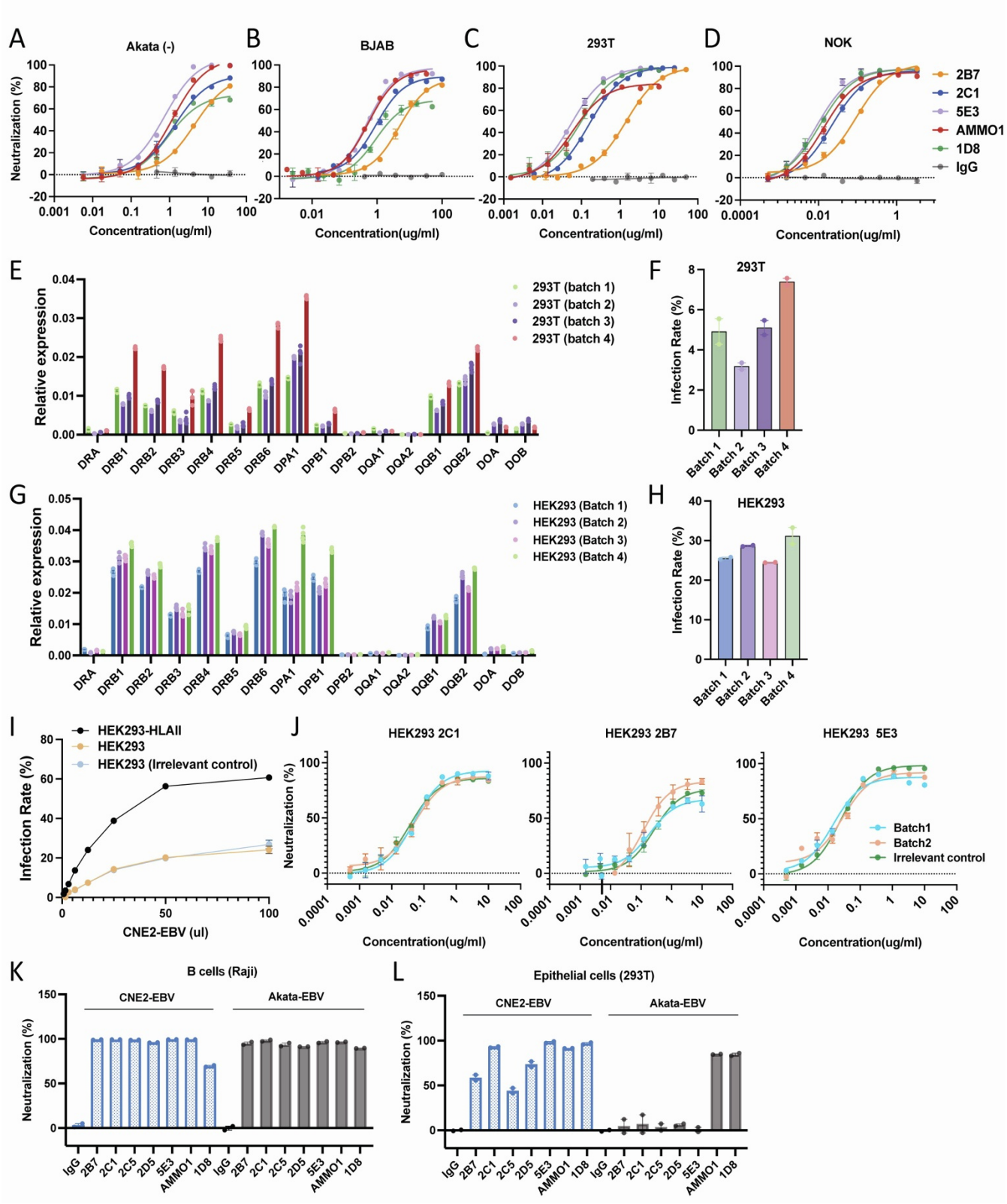

Figure S2. Neutralization effect of anti-gp42 antibodies in B and epithelial cells. Related to Figure 2.

(A-D) Neutralization assays evaluating the inhibitory effects of 2B7, 2C1, 5E3, AMMO1(anti-gH/gL), 1D8(anti-gH/gL), and control IgG in EBV-negative Akata B cell lines(A), BJAB B cell lines (B), 293T cell lines(C), and NOK cell lines(D). (n=3).

(E)Quantitative PCR (QPCR) analysis of human leukocyte antigen (HLA)-II gene expression in different batches of 293T cells. The expression levels are presented as relative fold changes to the GAPDH gene. (n=4).

(F) Assessment of CNE2-EBV infection rate in various batches of 293T cells. Equal amounts of CNE2-EBV were added to each cell. (n=2).

(G) QPCR analysis of HLA-II gene expression in various batches of HEK293 cells. The expression levels presented as relative fold change to the GAPDH gene. (n=4).

(H) Evaluation of CNE2-EBV infection rate in various batches of HEK293 cells. Equal amounts of CNE2-EBV were added to each cell. (n=2).

(I) Infection rate of HEK293 and HEK293-HLAII cells with varying volumes of CNE2-EBV supernatants. HEK293 (irrelevant control) represents HEK293 cells transfected with an irrelevant protein (T7 promoter). (n=3).

(J) Evaluation of the neutralizing efficacies of 2B7, 2C1, and 5E3 against EBV infection in different batches of HEK293 cells and HEK293 transfected with an irrelevant protein. (n=3).

(K-L) The neutralization ability of mAbs on CNE2-EBV or Akata-EBV infection was evaluated in Raji B cells (K) and 293T epithelial cells (L). 1 μg/ml mAb was added in each well. (n=2).

Error bars represent ± SEM.

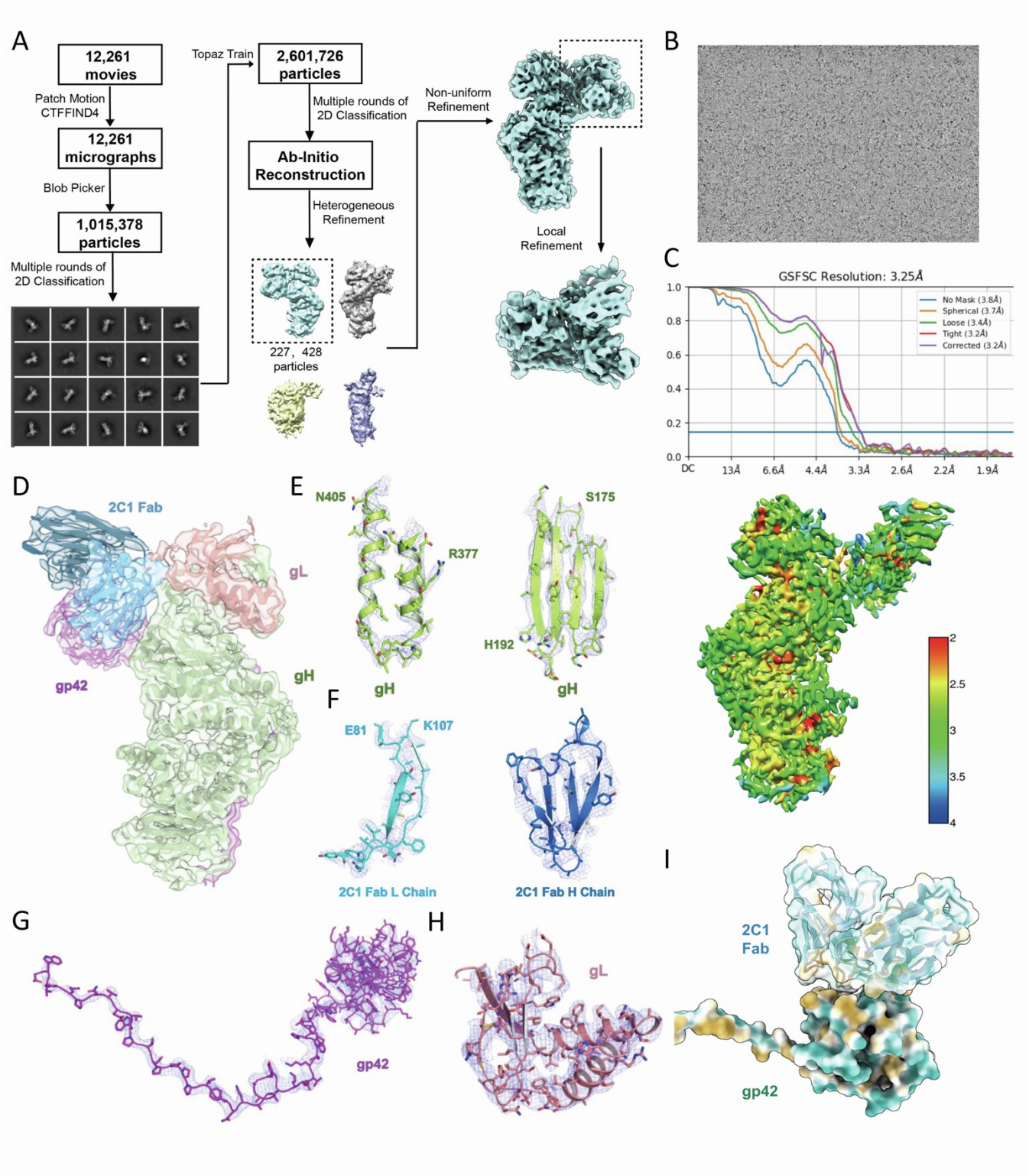

Figure S3. Cryo-EM Image Processing and Structural Analysis of EBV gH/gL/gp42/2C1-Fab Complex. Related to Figure 3.

(A) An overview of the cryo-EM image processing and reconstruction workflow.

(B) Representative cryo-EM micrograph of the gH/gL/gp42-2C1 Fab.

(C) The FSC curves for the reconstruction (upper) and Cryo-EM map of EBV gH/gL/gp42/2C1-Fab, colored by local resolution (Å) (lower).
(D) Overview of the gH/gL/gp42-2C1 Fab complex fitting into the cryo-EM density map. gH, gL, gp42, 2C1 fab heavy chain, and 2C1 fab light chain are colored green, salmon, purple, dark blue, and light blue, respectively;
(E-H) Detailed views showing the fit of side chains from different subunits into the corresponding cryo-EM volumes.
(I) Hydrophobic protein surface representation of 2C1 fab and EBV gp42, hydrophilic amino acids are colored blue, and hydrophobic amino acids are colored yellow.

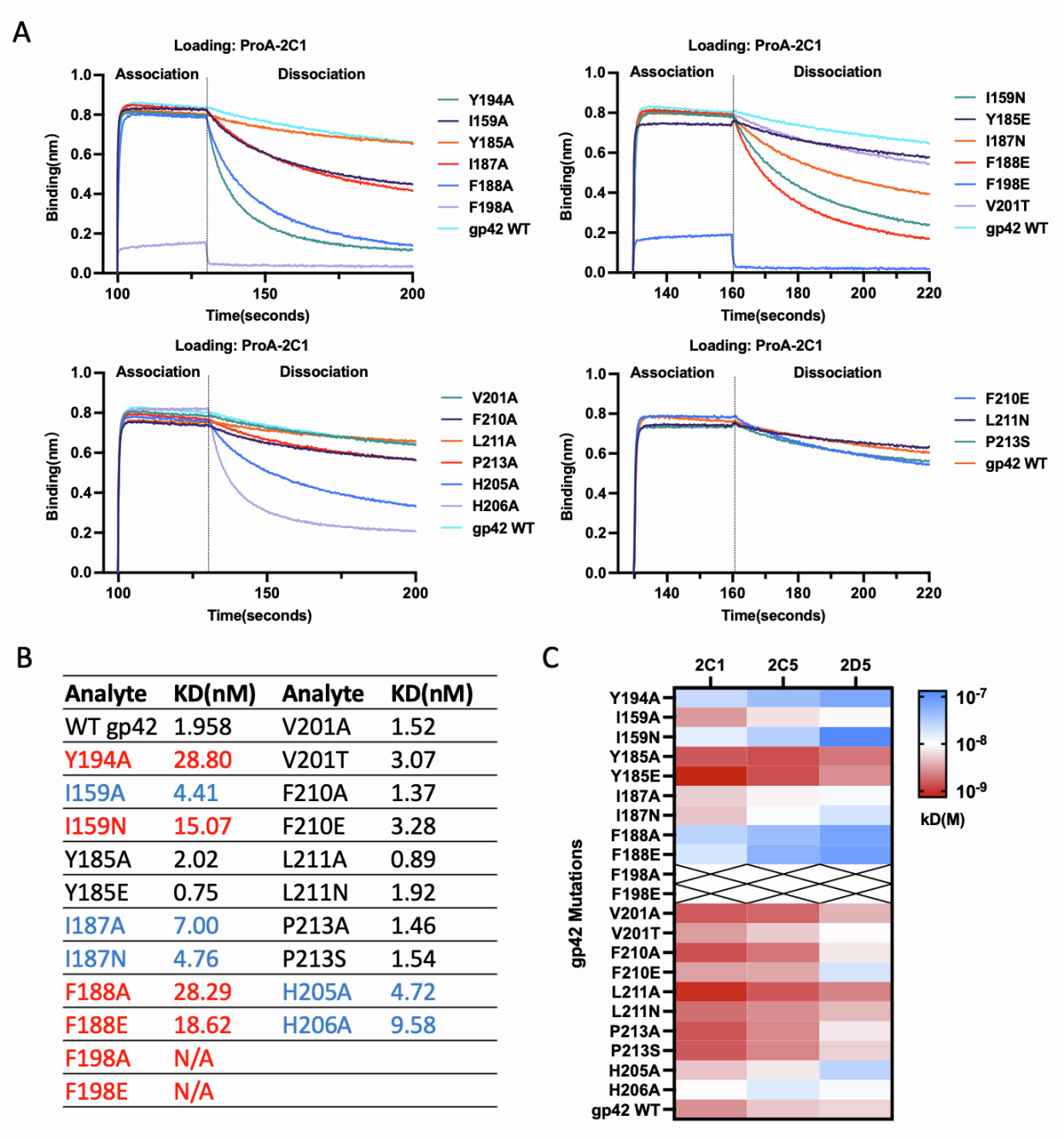

Analyte	KD(nM)	Analyte	KD(nM)
WT gp42	1.958	V201A	1.52
Y194A	28.80	V201T	3.07
I159A	4.41	F210A	1.37
I159N	15.07	F210E	3.28
Y185A	2.02	L211A	0.89
Y185E	0.75	L211N	1.92
I187A	7.00	P213A	1.46
I187N	4.76	P213S	1.54
F188A	28.29	H205A	4.72
F188E	18.62	H206A	9.58
F198A	N/A		
F198E	N/A		

Figure S4. Characterization of apparent affinity changes of 2C1 to gp42 mutants. Related to Figure 3.

(A) 2C1 was immobilized on Protein A sensors, and the apparent affinity of 2C1 to various gp42 mutants was assessed by BLI. WT refers to the wide-type gp42.

(B) The dissociation constant (kD) values corresponding to the apparent affinities of 2C1 to gp42 mutations, determined based on BLI data (average of two independent assays). Values are reported in nanomolar (nM). Mutations with the most significant effects on affinity (>10nM) are labeled in red, while moderately affected mutations (4~10nM) are labeled in blue.

(C) The heatmap represents variations in the apparent affinity (kD) of 2C1, 2C5, and 2D5 to gp42 caused by amino acid substitutions in gp42.

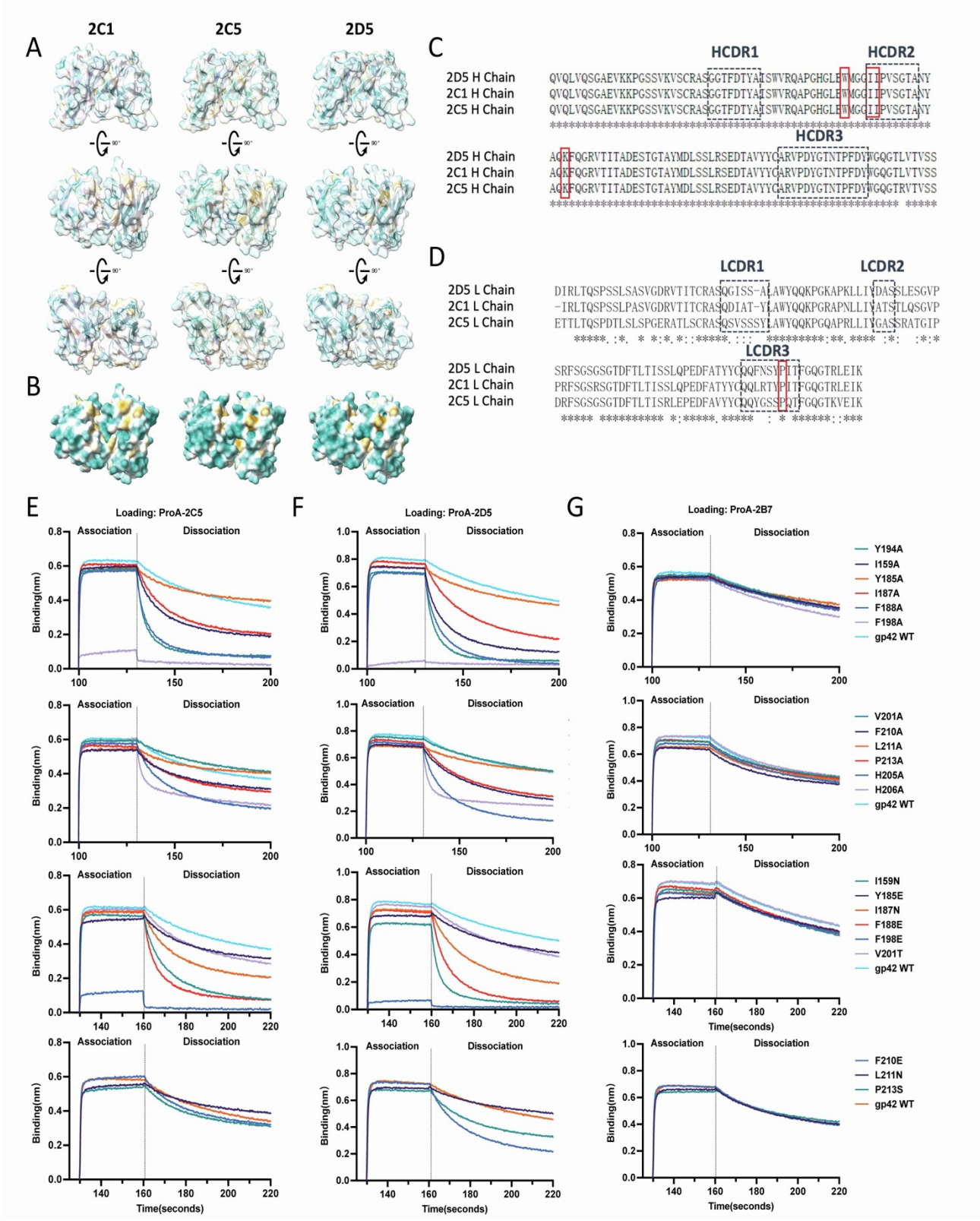

Figure S5. Prediction models of 2C1, 2C5, and 2D5 Fabs and Assessment of Apparent Affinity. Related to Figure 3.

(A) Prediction models of 2C1, 2C5, and 2D5 Fabs are shown in three different views, and CDRs of the VL are colored differently. The hydrophobic surface is indicated by yellow for hydrophobic amino acids and blue for hydrophilic amino acids, displayed as semi-transparent surfaces. Structures are predicted by tFold-Ab [S1]. (B) The hydrophobic surface of 2C1, 2C5, and 2D5 Fabs viewed from the gp42 interaction surface. (C) Sequence alignment of the heavy chains of 2C1, 2C5, and 2D5. The CDRs were labeled in black frames, and the conserved residues within the hydrophobic pockets of the interaction surface are highlighted in red frames. (D) Sequence alignment of the light chains of 2C1, 2C5, and 2D5, highlighting the conserved residue within the hydrophobic pockets. (E-G) 2C5(E), 2D5(F), and 2B7(G) mAbs were immobilized on Protein A sensors, followed by interacting with various gp42 mutants to assess their apparent affinity using bio-layer interferometry(BLI).

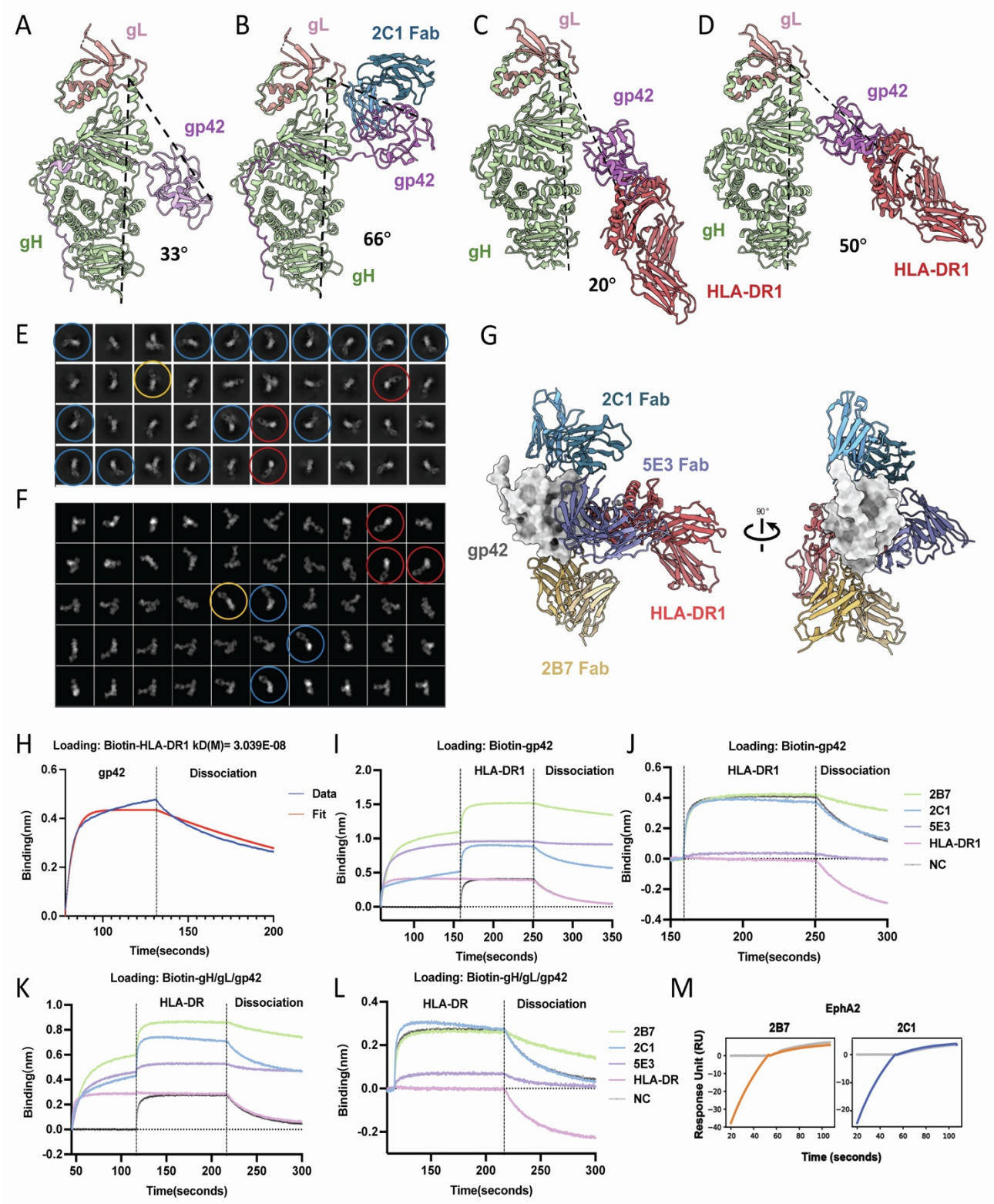

Figure S6. 2B7 and 2C1 antibodies reveal two distinct sites on gp42. Related to Figure 4.

(A) The crystal structure of the gH/gL/gp42 complex (PDB: 5T1D) reveals an angle of approximately 33° between gp42 (purple) and gH/gL (green and salmon).

(B) The Angle between gp42 and gH/gL in the structure of gH/gL-gp42-2C1 Fab complex is about 66°. The structure of EBV gp42, gH, gL, and 2C1 Fab are colored purple, green, salmon, and blue, respectively.
(C-D) Two different conformations of the gH/gL-gp42-HLA complex: closed (C) and open (D). The angles of gp42 and gH/gL in closed and open conformation are 20° and 50°, respectively. The crystal structure PDB of EBV gH/gL (green and salmon) and gp42 (purple)/HLA-DR1 (red) complex is 3PHF and 1KG0, respectively. (C-D) is adapted from [S2].
(E-F) The 2D classification results of gH/gL/gp42-2B7 Fab complex (E) and the projection of merged gH/gL/gp42-2B7 Fab model (F). Circles of the same color indicate projections of the same or similar orientation.
(G) Structure model of gp42(grey) in complex with HLA-DR1(red), 2C1 Fab (blue), 2B7 Fab (yellow), and 5E3 Fab (purple) [S3].
(H)Binding of gp42 to immobilized biotin-conjugated HLA-DR1 measured by BLI.
(I-J) Competition binding of 2B7, 2C1, or 5E3 with HLA-DR1 to immobilized gp42 was measured using bio-layer interferometry (BLI) (I). The binding shift was aligned at the HLA-DR1 loading step (158.8s) to visualize the competition (J).
(K-L) Competition binding of 2B7, 2C1, or 5E3 with HLA-DR1 to immobilized gH/gL/gp42 was assessed using BLI (K). To visualize the competition, the binding shift was aligned at the HLA-DR1 loading step (116.6s) (L).
(M) Competition binding of 2B7 or 2C1 with EphA2 to immobilized gH/gL/gp42 measured by Surface Plasmon Resonance (SPR).

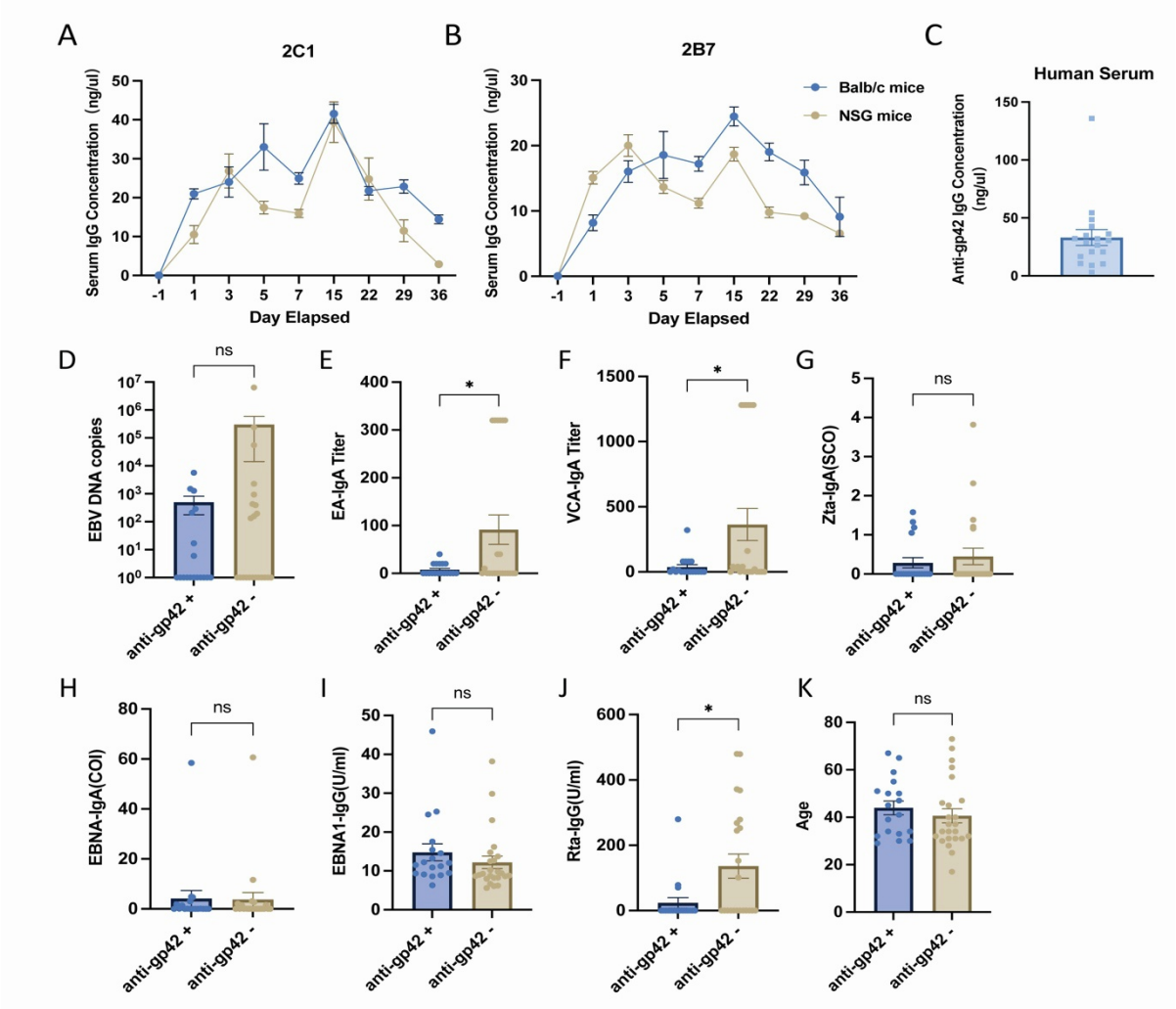

Figure S7. Evaluation of Antibody Concentrations in Mice and Human Serum. Related to Figures 5 and 7.

(A-B) Evaluation of mice serum concentration of 2C1 (A) and 2B7(B) using ELISA. Balb/c or NSG mice were administered 200 μg of mAbs intraperitoneally on days -1, 2, 7, and 14. The ELISA plates were coated with gp42 protein (100 ng/well), and purified 2C1 mAb was used as a quantitative control. (n=3).

(C) Measurement of gp42-specific antibody concentrations in serum from healthy virus carriers using ELISA. Gp42 protein was used for coating the ELISA plates(100ng/well), and purified 2C1 mAb was used as the quantitative control. (n=18).

(D-K) A comparison of various parameters between anti-gp42 positive (18/40) and anti-gp42 negative (22/40) EBV carriers. The data includes EBV DNA copies number (D), EA-IgA (E), VCA-IgA (F), Zta-IgA (G), EBNA1-IgA(H), EBNA1-IgG(I), Rta-IgG (J), and age (K) of the EBV carriers. SCO, Signal-to-Cut-off. COI, Cut-off index. The SCO and COI are calculated from the mean optical densities of the sample and Cut-off value (ODsample/standard). Human antibody detection was performed using an anti-human IgG HRP antibody (Abcam, ab97160).

Supplementary Table S1. Model statistics of gH/gL/gp42-2C1 structure. Related to Figure 3.

EBV gH/gL/gp42-2C1 map	
Data collection and processing	
Microscope	FEI Titan Krios
Camera	Gatan K3
Magnification	105,000
Voltage(kV)	300
Electron exposure (e^{-}/Å^2)	50
Defocus range (μm)	-1.0 ~ -2.0
Pixel size (Å)	0.855
Frames/movie	32
Movies (total)	12，193
Initial particle images (no.)	1,015,378
Final particle images (no.)	227，428
Symmetry imposed	C1
Map resolution (Å)	
FSC threshold	0.143
Map resolution range (Å)	2 - 6
Model composition	
Non-hydrogen atoms	8328
Protein residues	1138
Ligands	0
R.m.s. deviations	
Bond lengths (Å)	0.02
Bond angles (°)	0.536
Validation	
MolProbity score	1.87
Clashscore	7.38
Poor rotamers (%)	0.12
Ramachandran plot	
Favored (%)	92.6%
Allowed (%)	7.4%
Disallowed (%)	0

Supplementary Table S2. qPCR primers of HLA-II expression. Related to Figure 5.

HLA-II genes	Forward Primers	Reverse Primers
HLA-DRA	AGCTGTGGACAAAGCCAACCTG	CTCTCAGTTCCACAGGGCTGTT
HLA-DRB1	GAGCAAGATGCTGAGTGGAGTC	CTGTTGGCTGAAGTCCAGAGTG
HLA-DRB2	CTGTGAGTGGTTTCTATCCAGGC	CGAGGAACTGTTTCCAGCATCAC
HLA-DRB3	TTCCAGACCCTGGTGATGCTAG	GACTCCACTCAGCATCTTGCTC
HLA-DRB4	GCTGGAAACAGTTCCTCGGAGT	GACTCCACTCAGCATCTTGCTC
HLA-DRB5	GAACAGCCAGAAGGACTTCCTG	GCAGGATACACAGTCACCTTAGG
HLA-DRB6	CACGGACTGAATCTGCACAGAG	CTGTTGGCTGAAGTCCAGAGTG
HLA-DPA1	ATCCAGCGTTCCAACCACACTC	CGTTGAGCACTGGTGGGAAGAA
HLA-DPB1	GTGCAGACACAACTACGAGCTG	CCTGGGTAGAAATCCGTCACGT
HLA-DPB2	TGCGGCTCATATCTGTGGTCCA	CACTGCGCTGTCAAAATGCACG
HLA-DQA1	GCATTGTGGTGGGCACTGTCTT	TCTTCTGCTCCTGTAGATGGCG
HLA-DQA2	GAGACAGTCCAACTCTACCGCT	CCATTGCTCAGCCAGGTGATGT
HLA-DQB1	GAGCAAGATGCTGAGTGGCGTT	GTCTCAGGAGTCAGTGCAGAAG
HLA-DQB2	GTGTGCAGACACAACTACGAGG	TCACTGAGCAGACCAGCAGGTT
HLA-DOA	ATCGCCGCAATCAAAGCCCATC	TGCAGATGAGGATGTTGGGCTG
HLA-DOB	CCAGATGCTGAGCAGTGGAACA	GGTACACTGTCACCTCTGGTTG

HLA: Human leukocyte antigen.

SUPPLEMENTAL REFERENCES

S1. Wu, J., Wu, F., Jiang, B., Liu, W., and Zhao, P. (2022). tFold-Ab: Fast and Accurate Antibody Structure Prediction without Sequence Homologs. Preprint at bioRxiv, 10.1101/2022.11.10.515918 10.1101/2022.11.10.515918.

S2. Sathiyamoorthy, K., Jiang, J., Hu, Y.X., Rowe, C.L., Möhl, B.S., Chen, J., Jiang, W., Mellins, E.D., Longnecker, R., Zhou, Z.H., et al. (2014). Assembly and Architecture of the EBV B Cell Entry Triggering Complex. PLoS Pathog 10, e1004309. 10.1371/journal.ppat.1004309.

S3. Hong, J., Zhong, L., Liu, L., Wu, Q., Zhang, W., Chen, K., Wei, D., Sun, H., Zhou, X., Zhang, X., et al. (2023). Non-overlapping epitopes on the gHgL-gp42 complex for the rational design of a triple-antibody cocktail against EBV infection. Cell Rep Med 4, 101296. 10.1016/j.xcrm.2023.101296.